Oncogene (2013) 32, 27–38

www.nature.com/onc

ORIGINAL ARTICLE

Structural basis for the altered drug sensitivities of non-small cell lung cancer-associated mutants of human epidermal growth factor receptor

S Yoshikawa[1], M Kukimoto-Niino[1], L Parker[1], N Handa[1], T Terada[1], T Fujimoto[1], Y Terazawa[1], M Wakiyama[1], M Sato[2], S Sano[2], T Kobayashi[2], T Tanaka[2], L Chen[3], Z-J Liu[3,8], B-C Wang[3], M Shirouzu[1], S Kawa[4,9], K Semba[5], T Yamamoto[4,6] and S Yokoyama[1,7]

[1]RIKEN Systems and Structural Biology Center, Yokohama Institute, Yokohama, Japan; [2]Japan Aerospace Exploration Agency, Ibaraki, Japan; [3]Department of Biochemistry and Molecular Biology, University of Georgia, Athens, GA, USA; [4]Division of Oncology, The Institute of Medical Science, The University of Tokyo, Tokyo, Japan; [5]Department of Life Science & Medical Bioscience, School of Advanced Science and Engineering, Waseda University, Tokyo, Japan; [6]Cell Signal Unit, Okinawa Institute of Science and Technology, Okinawa, Japan and [7]Department of Biophysics and Biochemistry, Graduate School of Science, The University of Tokyo, Tokyo, Japan

The epidermal growth factor receptor (EGFR) has an essential role in multiple signaling pathways, including cell proliferation and migration, through extracellular ligand binding and subsequent activation of its intracellular tyrosine kinase (TK) domain. The non-small cell lung cancer (NSCLC)-associated EGFR mutants, L858R and G719S, are constitutively active and oncogenic. They display sensitivity to TK inhibitors, including gefitinib and erlotinib. In contrast, the secondary mutation of the gatekeeper residue, T790M, reportedly confers inhibitor resistance on the oncogenic EGFR mutants. In this study, our biochemical analyses revealed that the introduction of the T790M mutation confers gefitinib resistance on the G719S mutant. The G719S/T790M double mutant has enhanced activity and retains high gefitinib-binding affinity. The T790M mutation increases the ATP affinity of the G719S mutant, explaining the acquired drug resistance of the double mutant. Structural analyses of the G719S/T790M double mutant, as well as the wild type and the G719S and L858R mutants, revealed that the T790M mutation stabilizes the hydrophobic spine of the active EGFR-TK conformation. The Met790 side chain of the G719S/T790M double mutant, in the apo form and gefitinib- and AMPPNP-bound forms, adopts different conformations that explain the accommodation of these ligands. In the L858R mutant structure, the active-site cleft is expanded by the repositioning of Phe723 within the P-loop. Notably, the introduction of the F723A mutation greatly enhanced the gefitinib sensitivity of the wild-type EGFR *in vivo*, supporting our hypothesis that the expansion of the active-site cleft results in enhanced gefitinib sensitivity. Taken together, our results provide a structural basis for the altered drug sensitivities caused by distinct NSCLC-associated EGFR mutations.

Oncogene (2013) **32,** 27–38; doi:10.1038/onc.2012.21; published online 20 February 2012

Keywords: EGFR; T790M; gefitinib; tyrosine kinase inhibitor; NSCLC; drug resistance

Introduction

The human epidermal growth factor receptor (EGFR) is a multidomain protein composed of an extracellular ligand-binding domain, a single transmembrane domain and an intracellular tyrosine kinase (TK) domain. Stimulation of the receptor with EGF or other cognate ligands induces receptor homo- or heterodimerization and autophosphorylation of key Tyr residues within the carboxy terminal portion of the receptor. These phosphorylated Tyr residues serve as the binding sites for several signal transducers that initiate multiple signaling pathways, including those resulting in cancer phenotypes (Arteaga, 2002).

Gefitinib (Iressa) is an orally active TK inhibitor (TKI) that blocks signal transduction pathways implicated in cancers (Wakeling *et al*., 2002). Tumors from non-small cell lung cancer (NSCLC) patients with favorable clinical responses to the TKIs, such as gefitinib, erlotinib and lapatinib, have been shown to contain EGFR somatic activating mutations (Lynch *et al*., 2004; Paez *et al*., 2004; Pao *et al*., 2004). The most frequent mutation is a point substitution within the activation loop (A-loop) that replaces Leu858 with Arg (L858R). The mutation within the phosphate-binding loop (P-loop) that replaces Gly719 with Ser (G719S) is found less frequently (Shigematsu and Gazdar, 2006). Cells bearing the mutant EGFR proteins display oncogenic properties, but are generally more sensitive

Correspondence: Professor S Yokoyama, RIKEN Systems and Structural Biology Center, Yokohama Institute, 1-7-22 Suehiro-cho, Yokohama 230-0045, Japan
E-mail: yokoyama@biochem.s.u-tokyo.ac.jp or Professor T Yamamoto, Division of Oncology, The Institute of Medical Science, The University of Tokyo, 4-6-1 Shirokanedai, Minato-ku, Tokyo 108-8639, Japan
E-mail: tyamamot@ims.u-tokyo.ac.jp
[8]Present address: National Laboratory of Biomacromolecules, Institute of Biophysics, Chinese Academy of Sciences, Beijing 100101, China
[9]Present address: Laboratory of Molecular Biology, National Cancer Institute, NIH, Bethesda, MD 20892, USA
Received 16 April 2010; revised 29 October 2011; accepted 6 January 2012; published online 20 February 2012

to inhibitors than cells expressing the wild-type EGFR protein. In particular, the L858R mutant is 10- to 100-fold more sensitive to erlotinib and gefitinib than the wild-type EGFR (Pao *et al*., 2004; Greulich *et al*., 2005; Mukohara *et al*., 2005) and significantly more sensitive than the G719S mutant (Jiang *et al*., 2005). *In vitro* kinetic analyses revealed that the L858R and G719S mutants display higher enzymatic activity, and that the L858R mutant has greater TKI-binding affinity, as compared with the wild-type EGFR-TK (Yun *et al*., 2007). The structures of the L858R and G719S mutants complexed with either AMPPNP or the inhibitors, gefitinib and AEE788, revealed that the overall conformation and ligand-binding modes are very similar to those of the wild-type EGFR-TK in the active conformation (Yun *et al*., 2007).

NSCLC patients who initially respond to TKIs, but subsequently relapse, often have a secondary T790M mutation, which results in acquired drug resistance (Kobayashi *et al*., 2005; Pao *et al*., 2005). This Thr residue is known as the 'gatekeeper', which controls the access of the inhibitors to a deep hydrophobic pocket in the ATP-binding site (Liu *et al*., 1998). It was first predicted that the T790M mutation sterically hindered the binding of TKIs to the EGFR kinase domain, by the introduction of a bulky Met residue, thus resulting in drug resistance (Kobayashi *et al*., 2005; Pao *et al*., 2005). A recent report, however, directly showed that the T790M mutant binds gefitinib ~8-fold more tightly than the wild type. Indeed, the structure of the T790M mutant revealed that the Met790 residue can shift to accommodate the binding of inhibitors, such as AEE788 and HKI-272 (Yun *et al*., 2008). The authors also found that the secondary T790M mutation greatly increased the ATP-binding affinity of the L858R mutant. They suggested that the clinically observed TKI resistance associated with the secondary T790M mutation is not attributable to steric blocking of inhibitor binding, as previously hypothesized, but rather to the enhanced affinity for ATP, although its binding mode was not clarified by the previously reported structures. The analogous gatekeeper mutation is found in many protein kinases that are implicated in cancer (Dixit *et al*., 2009). The structural analysis of the c-SRC mutant (T334I) revealed that the gatekeeper mutation activates the kinase by stabilizing the 'hydrophobic spine', which is characteristic of the active kinase conformations (Azam *et al*., 2008). A similar mechanism of activation was proposed by computational modeling of the EGFR T790M mutant (Azam *et al*., 2008).

The development of specific inhibitors to target drug-resistant EGFR mutants has become an important focus for the pharmaceutical management of NSCLC patients. Recently, novel inhibitors with increased selectivity against the EGFR T790M mutant have been identified (Engelman *et al*., 2007; de La Motte Rouge *et al*., 2007; Li *et al*., 2008; Cha *et al*., 2009, 2011; Zhou *et al*., 2009, 2011; Carmi *et al*., 2010; Wu *et al*., 2010; Kobayashi *et al*., 2012; Taube *et al*., 2011).

In this study, we characterized the biochemical properties of the EGFR G719S/T790M double mutant. We confirmed that the G719S/T790M double mutant acquires resistance to gefitinib, with increased kinase activity and ATP affinity, as in the case of the previously characterized L858R/T790M double mutant (Yun *et al*., 2008). We also determined the crystal structures of the G719S/T790M double mutant and the wild type and two drug-sensitive mutants, G719S and L858R, for direct comparison. The structures revealed the essential role of the Met790 side chain in the stabilization of the active conformation, as well as in the accommodation of AMPPMP or gefitinib in the binding site. We also observed a novel P-loop conformation in the L858R mutant, where the repositioning of the Phe723 residue results in the expansion of the active-site cleft. Structure-based mutagenesis of the full-length EGFR revealed that the expansion of the active-site cleft by the F723A mutation resulted in a significant increase in gefitinib sensitivity.

Results

In vitro *study*

Inhibitory potency and binding ability of gefitinib. The T790M mutation reportedly confers resistance to gefitinib or erlotinib on the oncogenic EGFR mutants (L858R and del L747-E749; A750P), which are usually sensitive to these drugs (Pao *et al*., 2005). To further examine the effect of the secondary T790M mutation, we determined the IC_{50} (half maximal inhibitory concentration) value of the G719S/T790M double mutant EGFR-TK domain and compared its gefitinib sensitivity with those of the wild-type and G719S

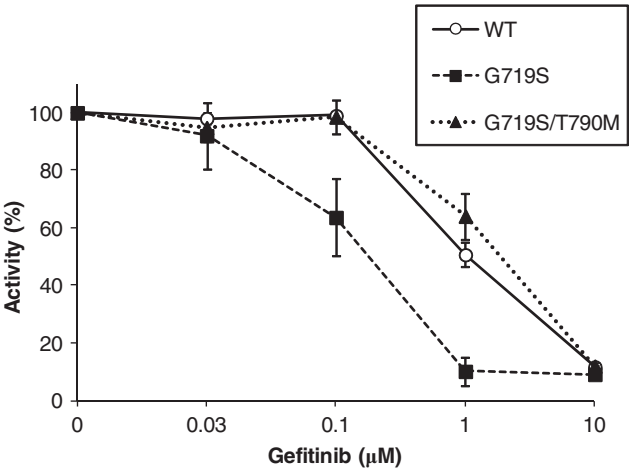

EGFR kinase	IC_{50} value
WT	1.04 μM
G719S	0.18 μM
G719S/T790M	1.86 μM

Figure 1 The T790M secondary mutation of the G719S mutant confers resistance to gefitinib. The wild-type (circles) and the G719S (squares) and G719S/T790M (triangles) mutant EGFR kinases were assayed to measure the inhibitory effects of gefitinib at the indicated concentrations. The activities of the kinases in the absence of gefitinib were set to 100. Error bars indicate s.d.

Table 1 X-ray data collection and refinement statistics for the G719S/T790M mutant

Structure	*G719S/T790M apo form*	*G719S/T790M + gefitinib*	*G719S/T790M + AMPPNP*
Data collection			
Beamline	BL41XU (SPring-8)	BL26B2 (SPring-8)	BL41XU (SPring-8)
Space group	I23	I23	I23
Unit-cell parameters $a=b=c$ Å)	141.3	143.5	144.0
Wavelength (Å)	1.0	1.0	1.0
Resolution (Å)	2.75 (2.90–2.75)	2.50 (2.64–2.50)	2.34 (2.42–2.34)
Unique reflections	12348	17240	21045
Redundancy	5.1 (5.1)	45.3 (45.7)	7.3 (7.1)
Completeness (%)	99.9 (100.0)	100.0 (100.0)	99.9 (100.0)
I/σ (I)	6.5 (1.8)	5.7 (1.7)	25.8 (3.8)
R_{sym}[a] (%)	8.8 (41.9)	9.3 (44.9)	6.1 (55.8)
Refinement			
Resolution (Å)	50.00–2.75	45.45–2.50	38.47–2.34
No. of reflections	12334	17208	20399
No. of protein atoms	2385	2408	2378
No. of ligand atoms	0	31	31
No. of water molecules	13	55	30
R_{work} (%)	19.6	18.6	19.7
R_{free} (%)[b]	24.3	24.9	24.4
r.m.s.d. bond length (Å)	0.018	0.025	0.010
r.m.s.d. bond angles (°)	1.8	2.2	1.5
Ramachandran plot			
Favored regions (%)	92.7	95.9	96.5
Allowed regions (%)	97.6	99.0	100.0
Outliers (%)	2.4	1.0	0.0
PDB code	3ug1	3ug2	3vjn

Abbreviation: PDB, Protein Data Bank.
All numbers in parentheses represent last outer shell statistics.
[a]$R_{sym}=\Sigma|I_{avg}-I_i|/\Sigma I_i$, where I_i is the observed intensity and I_{avg} is the average intensity.
[b]R_{free} is calculated for 10% of randomly selected reflections excluded from refinement.

mutant proteins (Figure 1). Consistent with the previous reports, the G719S mutant was more sensitive to gefitinib ($IC_{50}=0.18\,\mu M$) than the wild-type protein ($IC_{50}=1.04\,\mu M$). In contrast, the G719S/T790M double mutant was ~10-fold less sensitive to gefitinib ($IC_{50}=1.86\,\mu M$) as compared with the G719S mutant. Therefore, the T790M mutation effectively enhances the drug resistance of the G719S mutant. The acquired drug resistance of the G719S/T790M double mutant is not attributed to the reduced binding of gefitinib, because the G719S/T790M double mutant bound gefitinib with a $K_d=5.6\,nM$, which is tighter than G719S ($K_d=31.9\,nM$) and the wild type ($K_d=14.2\,nM$; Table 3).

Kinetic analysis. We studied the *in vitro* kinetics of the wild-type and mutant EGFR-TK domains (Table 3). The G719S/T790M double mutant showed a 2.2-fold. increase in the kinase activity (k_{cat}), while the G719S mutant showed a 5.9-fold increase, as compared with the wild type (Table 3). The G719S mutant has a higher Michaelis–Menten constant (K_m; 13.3-fold) for ATP, as compared with the wild type, which is consistent with the previous report (Yun *et al*., 2007). In contrast, the K_m value of the G719S/T790M double mutant is lower than that of the G719S mutant, and closer to that of the wild type. The results indicated that the secondary T790M mutation effectively restores the nucleotide-binding ability of the G719S mutant, as in the case of the L858R mutant (Yun *et al*., 2007).

Structure determination. To explore the structural basis for the acquired drug resistance, we determined the crystal structures of the G719S/T790M double mutant EGFR-TK domain in the apo form, and complexed with gefitinib and AMPPNP (Table 1). For direct comparison, we also determined the structures of the wild-type, G719S and L858R EGFR-TK domains crystallized in the presence of AMPPNP (Table 2). The wild-type and L858R structures were refined as complexes with AMPPNP, whereas AMPPNP was not included in the G719S structure, because of its weak electron density. The P-loop is partially disordered in all of the structures, albeit to different extents (residue 721 for L858R, residues 721–722 for the wild type, and residues 721–723 for G719S and G719S/T790M). The A-loop was also disordered in the G719S and L858R mutant structures (residue 865 for G719S and residues 862–875 for L858R), whereas in the wild-type and G719S/T790M double mutant structures, the A-loop was well ordered. The temperature-factor profiles indicated high flexibility for these loop regions of the molecule, but the G719S/T790M and G719S mutants have lower temperature factors for the P-loop, as compared with the wild type. This indicates the reduced P-loop flexibility caused by the G719S mutation within this loop.

Overall structures. The structures of the G719S/T790M double mutant, like those of the wild type,

Table 2 X–ray data collection and refinement statistics for the wild type and other mutants

Structure	*Wild type + AMPPNP*	*G719S*	*L858R + AMPPNP*
Data collection			
Beamline	X06SA (SLS)	22-ID (APS)	BL-5A (PF)
Space group	I23	I23	I23
Unit-cell parameters			
$a = b = c$ (Å)	143.4	145.5	144.7
Wavelength (Å)	0.9786	0.97243	1.0
Resolution (Å)	2.64 (2.74–2.64)	2.50 (2.59–2.50)	2.84 (2.94–2.84)
Unique reflections	14516	17866	12050
Redundancy	6.7 (6.9)	43.1 (33.3)	29.4 (29.9)
Completeness (%)	99.7 (99.8)	100.0 (100.0)	100.0 (100.0)
I/σ (I)	30.2 (6.5)	35.4 (9.8)	53.8 (5.8)
R_{sym}[a] (%)	4.2 (20.8)	13.7 (48.4)	8.7 (81.4)
Refinement			
Resolution (Å)	45.34–2.64	46.00–2.50	36.17–2.84
No. of reflections	14505	17863	11733
No. of protein atoms	2382	2443	2365
No. of ligand atoms	31	0	31
No. of water molecules	9	16	1
R_{work} (%)	19.0	19.8	19.0
R_{free} (%)[b]	22.8	25.3	23.6
r.m.s.d. bond length (Å)	0.010	0.010	0.010
r.m.s.d. bond angles (°)	1.8	1.5	1.6
Ramachandran plot			
Favored regions (%)	95.5	93.9	89.2
Allowed regions (%)	100.0	99.0	97.9
Outliers (%)	0.0	1.0	2.1
PDB code	3vjo	2eb2	2eb3

Abbreviation: PDB, Protein Data Bank.
All numbers in parentheses represent last outer shell statistics.
[a]$R_{sym} = \Sigma|I_{avg} - I_i|/\Sigma I_i$, where I_i is the observed intensity and I_{avg} is the average intensity.
[b]R_{free} is calculated for 10% of randomly selected reflections excluded from refinement.

G719S and L858R, adopt an active conformation (Figure 2). Leu777, Met766, Phe856 and His835 form a network of hydrophobic interactions from the N-lobe via the active site to the activation loop, termed the 'hydrophobic spine', which characterizes the active kinase conformation (Kornev *et al*., 2006). The T790M gatekeeper mutation is located in the hinge region between the N- and C-lobes. In the present structures of the G719S/T790M double mutant, the gatekeeper Met790 is situated at the top of the hydrophobic spine and stabilizes it in the active conformation (Figure 2). This structural feature accounts for the increased activity of this mutant.

Effect of the G719S mutation on AMPPNP binding. The G719S mutation is located within the P-loop at the first Gly residue in the conserved 'GXGXXG' sequence motif. In the crystal structure of the G719S/T790M double mutant with AMPPNP, the electron density for the AMPPNP ligand was clearly observed in the ATP-binding pocket (Figure 3a). A superposition of the G719S/T790M–AMPPNP complex onto the wild-type–AMPPNP complex revealed some differences, including a slight upward shift of the P-loop (Figure 3b).

On the other hand, the electron density for the entire AMPPNP molecule was not obtained in the ATP-binding pocket of the G719S single mutant (Figure 3c). The residual electron density in this site is probably due to the partial disorder of the AMPPNP ligand. The position of the P-loop in the G719S single mutant is almost the same as that observed in the G719S/T790M double mutant (Figure 3c), suggesting that this G719S mutation is responsible for this upward shift of the P-loop in these mutants, as compared with the wild type (Figure 3b). These observations suggest that the G719S mutant may have reduced binding affinity for nucleotides, probably caused by the altered P-loop conformation, and that the secondary T790M mutation may counteract the reduction in the ATP-binding affinity caused by the primary G719S mutation.

Effect of the secondary T790M mutation of the G719S mutant. Interactions with AMPPNP. To determine how the secondary T790M mutation restores the ATP-binding affinity of the G719S mutant, we compared the AMPPNP-binding modes of the G719S/T790M double mutant with that of the wild type. AMPPNP is bound in a similar manner in both structures, where the adenine base hydrogen bonds with the backbones of Met793 and Gln791. However, in the G719S/T790M double mutant, the AMPPNP adopts a different position, which effectively shortens the hydrogen bond between the α

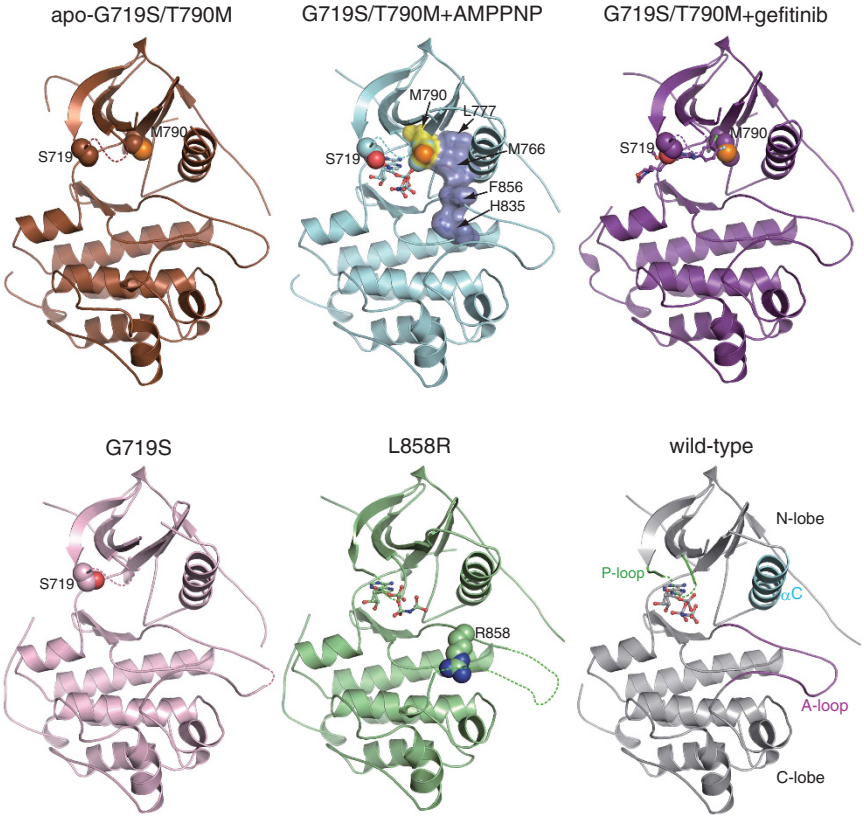

Figure 2 Overview of the crystal structures of the EGFR-TK domains, shown in cartoon representations with the apo G719S/T790M in brown, G719S/T790M complexed with AMPPNP in cyan, G719S/T790M complexed with gefitinib in purple, G719S in pink, L858R complexed with AMPPNP in green and the wild type complexed with AMPPNP in gray. The AMPNP molecule, which is missing in the G719S structure, is represented by a stick model. The residues Ser719, Met790 and Arg858 in the mutant EGFR-TK domains are shown as spheres. The surface projections of the hydrophobic residues in the G719S/T790M complexed with AMPPNP indicate the hydrophobic spine. The dashed lines indicate the disordered regions in the P-loop and A-loop.

phosphate and Asp855 and Lys745 (Figure 4a). At the gatekeeper position, the Met790 side chain in the G719S/T790M double mutant forms closer contacts with the adenine ring of AMPPNP, as compared with those made by the Thr790 side chain in the wild type (Figure 4c). In addition, this Met790 side chain in the double mutant significantly alters its conformation to optimize AMPPNP binding; in the AMPPNP-bound form, this side chain extends further into the ATP-binding pocket, as compared with that in the apo form (Figures 4b and c). Together, these findings revealed that a Met residue at the gatekeeper position is more favorable for the tight binding of AMPPNP than the Thr residue of the wild-type protein (Figure 4c).

Interactions with gefitinib. In the crystal structure of the gefitinib-bound form of the G719S/T790M double mutant, the Met790 side chain assumes a distinct conformation, as compared with its AMPPNP-bound form (Figure 4d). The conformations adopted by the Met790 residue in our G719S/T790M structures are also different from that in the previously reported T790M–AEE788 complex structure (Yun *et al*., 2008). This suggests that Met790 can optimize its conformation to suit the ligand bound in the pocket.

We also compared the gefitinib-binding modes of our G719S/T790M double mutant structure with that of the previously reported wild-type structure (PDB code: 2ity; Figure 4e). The main hydrogen bonds between the protein and inhibitor are common to both structures (between the quinazoline ring of gefitinib and the backbone NH of Met793, and between the aniline ring of gefitinib and the backbone oxygen of Leu788), but the aniline ring of the inhibitor in the double mutant has rotated upwards, as compared with its position in the wild-type structure. This shift is presumably an adaptation made by the inhibitor to adjust to the modified binding site of the G719S/T790M double mutant.

Characteristics of the L858R gefitinib sensitive mutant. The L858R substitution, which results in a significant increase in gefitinib sensitivity, is located at the N-terminal end of the A-loop. A comparison of the structures of the wild-type–AMPPNP complex and the L858R–AMPPNP complex revealed a conformational change of Phe723, which is located within the P-loop (Figure 5a). In the wild-type–AMPPNP complex structure, the side chain of Phe723 faces the β and γ phosphate groups of the bound AMPPNP, whereas in the L858R–AMPPNP complex, the Phe723 side chain is rotated upwards, thus making the binding site more accessible and possibly facilitating the release of the

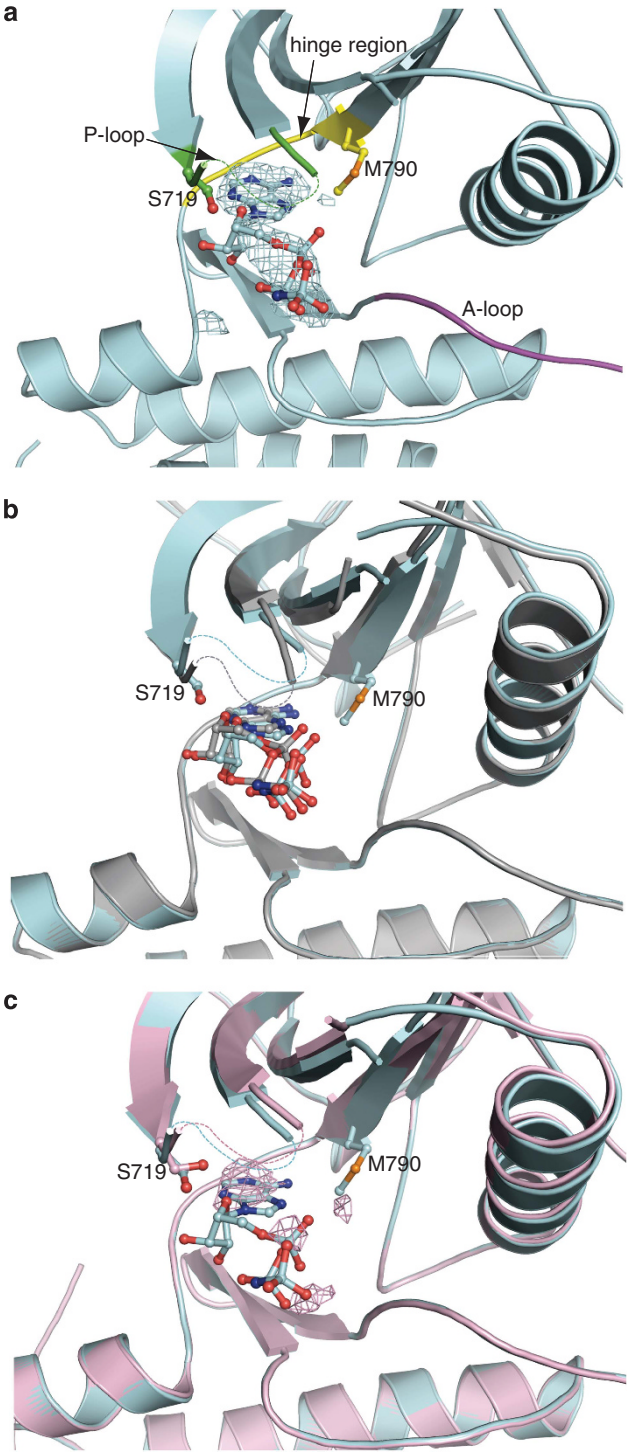

Figure 3 Close-up view of the AMPPNP-binding site. The G719S/T790M double mutant restores the affinity for ATP, as compared with the G719S mutant. (**a**) The structure of the G719S/T790M double mutant, shown together with the 2Fo–Fc electron density map (1σ) of the AMPPNP. The locations of the P-loop, A-loop and hinge region are shown in green, magenta and yellow, respectively. (**b**) The structure of the G719S/T790M mutant (cyan) superimposed on the wild-type EGFR-TK domain (gray) with their bound AMPPNP molecules. (**c**) The structure of the G719S/T790M mutant (cyan) with the bound AMPPNP superimposed on the G719S mutant (pink), shown together with the 2Fo–Fc electron density map (1σ) of the AMPPNP-binding site.

ATP molecule (Figure 5b). In the upwardly rotated conformation, Phe723 forms new interactions with Arg748 from the N-lobe (Figure 5a). A comparison with all of the other EGFR kinase structures in the PDB revealed that the position adopted by the Phe723 residue in our L858R–AMPPNP complex is unique. This novel conformation results in a wider and more accessible active-site cleft, which, we hypothesize, may be responsible for the increased drug sensitivity displayed by the L858R mutant. However, we cannot rule out the possibility that these structural changes are a result of the different conditions required for the crystallization of this specific mutant (see Materials and methods section for details).

In addition to the shift in the position of the Phe723 residue, we also observed a conformational change in the position of Arg858 in our structures, as compared with those reported previously (Yun *et al*., 2007). In the present L858R structure, the Arg858 residue now forms a hydrogen bond with the hydroxyl of Tyr891 (2.74 Å; Figure 5a), an interaction that is absent in all other previously reported L858R structures, with the exception of the L858R–gefitinib complex (Yun *et al*., 2007).

In the L858R mutant, the A-loop region is disordered, which may reflect the high level of mobility for this region. It is likely that this increased A-loop mobility could in turn affect the conformation of the P-loop, as in the inactive conformation Phe723 from the P-loop interacts with hydrophobic residues from the A-loop (including Leu858), displacing the αC helix from the active site (as seen in the wild-type–Lapatinib complex; PDB code: 1xkk; Wood *et al*., 2004; Figure 5c). On the basis of the inactive structure, it was previously proposed that the G719S and L858R mutations prevent the kinase from adopting the inactive conformation, because of the disruption of these stabilizing P-loop/A-loop interactions, resulting in a constitutively active form of the protein (Zhang *et al*., 2006; Yun *et al*., 2007). In addition, we hypothesize that the L858R mutant is stabilized in its active form through the formation of additional interactions, as observed in the L858R structure discussed above. Our L858R mutant structure revealed the formation of a hydrophobic interaction between a novel conformation of the Phe723 residue and Arg748, as well as an additional hydrogen bond between the mutated Arg858 residue and Tyr891.

Effect of the Phe723 mutation on the gefitinib sensitivities of EGFR. As the large Phe723 side chain hangs over the entrance of the active site in the wild-type EGFR-TK structure (Figure 5b), the substitution of Phe723 with Ala was expected to result in the expansion of the active-site cleft, thus conferring gefitinib sensitivity. To verify this hypothesis, we created a full-length EGFR mutant, in which Phe723 is replaced with Ala, and evaluated the effect of the mutation on the gefitinib sensitivity *in vivo*.

We examined the EGF-mediated autophosphorylation of EGFR and its mutants (F723A, L858R and G719S) with various concentrations of gefitinib, by a western blot analysis. As shown in Figure 6a, the

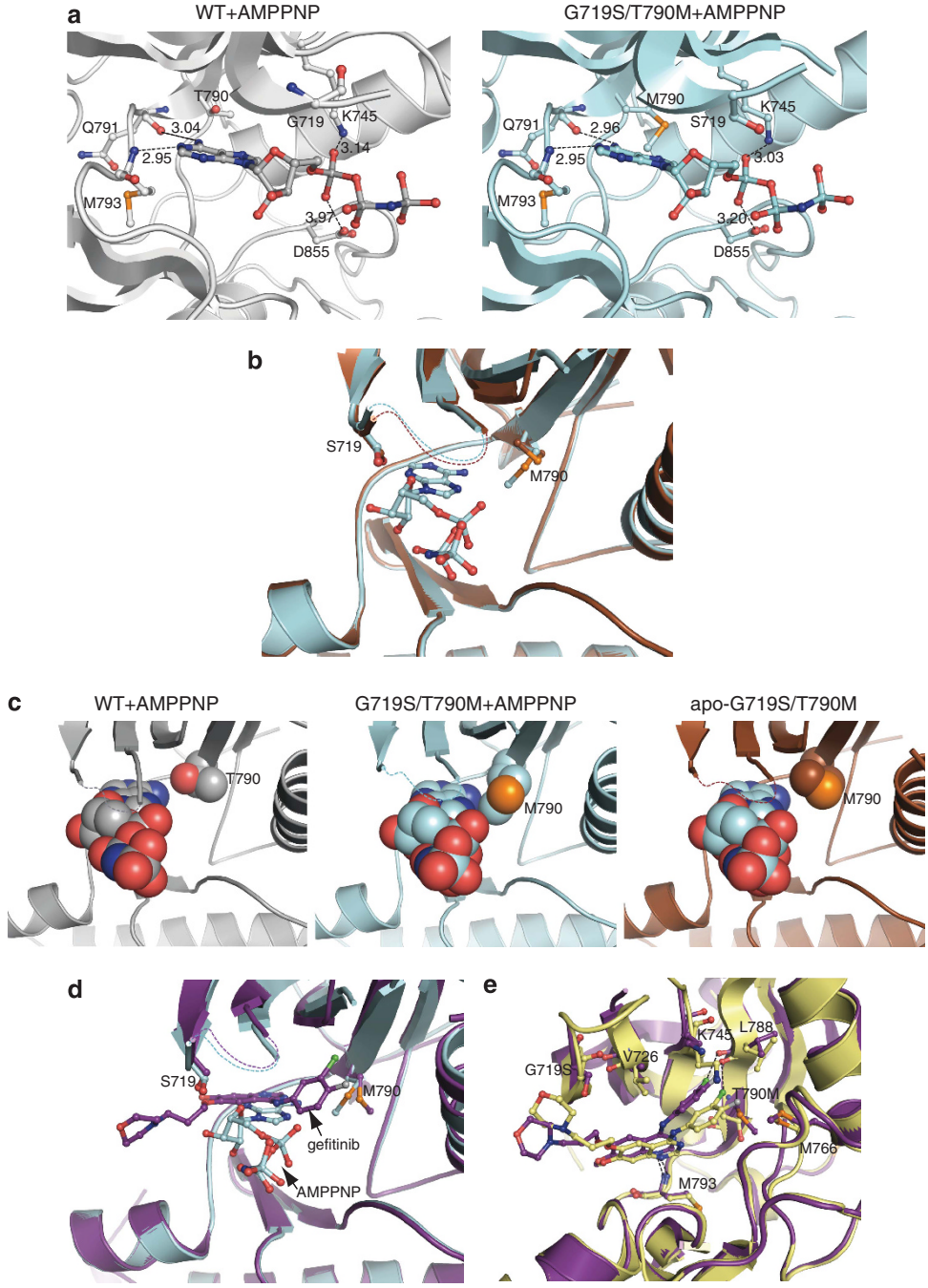

Figure 4 The T790M mutation contributes to the tight binding of AMPPNP, and its conformation changes depending on the bound ligand. (**a**) AMPPNP-binding modes in the wild-type (left) and G719S/T790M (right) EGFR-TK domains. Bond distances are indicated with dashed lines. Note the hydrogen bond between Asp855 and AMPPNP in the G719S/T790M mutant. (**b**) The structure of the G719S/T790M mutant complexed with AMPPNP (cyan), superposed on that of the apo G719S/T790M mutant (brown). The side-chain conformation of Met790 has shifted slightly to accommodate AMPPNP binding. (**c**) Comparison of the AMPPNP-binding sites of the wild type (left), the AMPPNP-bound G719S/T790M (middle) and the apo G719S/T790M (right). For comparison, the AMPPNP in the AMPPNP-bound G719S/T790M structure (middle) is also shown in the apo G719S/T790M structure (right). AMPPNP, Thr790 (wild type) and Met790 (G719S/T790M) are shown in sphere representations. The Met side chain interacts more snugly with AMPPNP, as compared with the interaction generated by the Thr side chain. The Met residue shifts closer to the AMPPNP in the AMPPNP-bound form, as compared with the apo form. (**d**) Superposition of the G719S/T790M mutant structures in the AMPPNP-bound form (cyan) and in the gefitinib-bound form (purple). The side-chain conformation of the Met790 residue has moved to accommodate gefitinib binding. (**e**) Superposition of the gefitinib-bound structures of the G719S/T790M mutant (purple) and the wild type (yellow). The Met790 substitution results in a rotation of the aniline ring of the gefitinib. Hydrogen bonds are indicated with dashed lines.

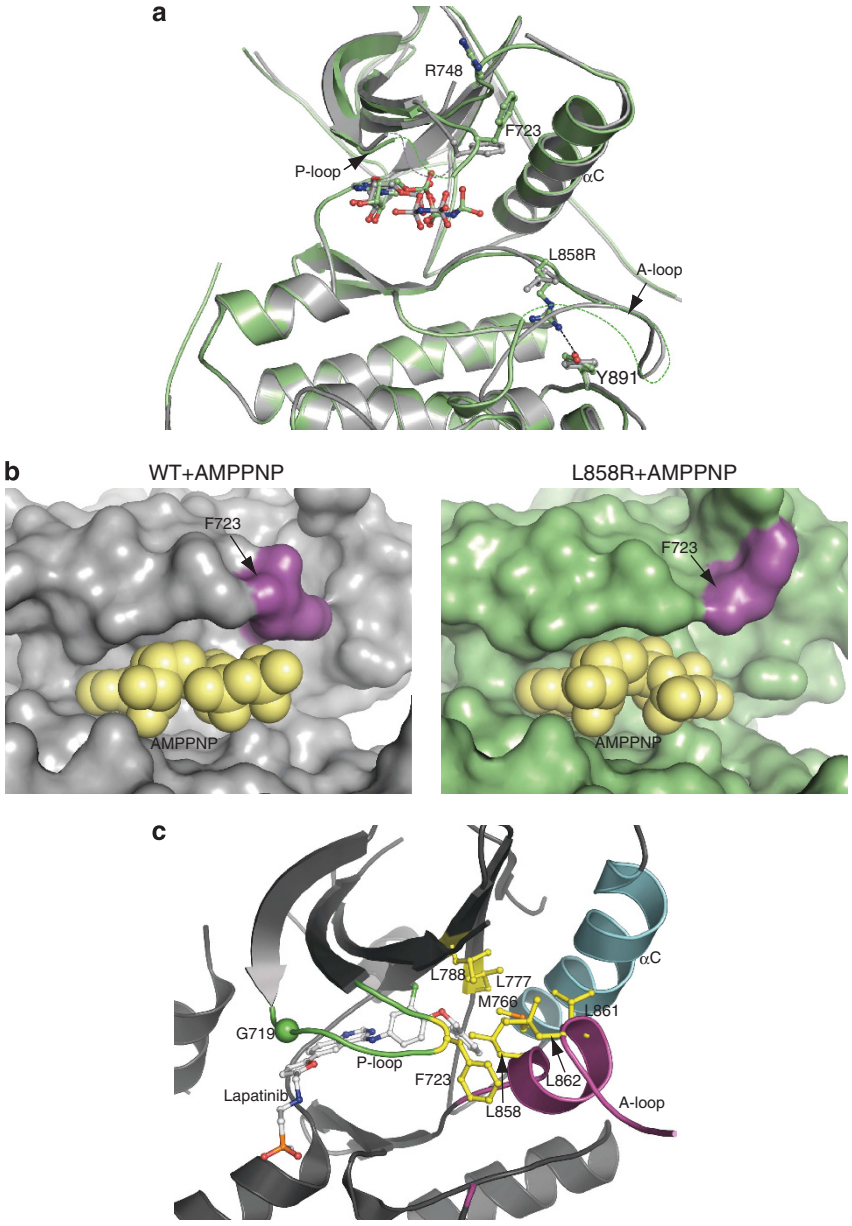

Figure 5 The L858R mutant displays increased A-loop mobility, and the Phe723 residue adopts a different conformation. (**a**) The structure of the L858R mutant (green) superposed on that of the wild type (gray). The dashed line indicates the hydrogen bond that is observed only in the L858R mutant. In the structure of the L858R mutant, the A-loop is highly disordered and the conformation of Phe723 in the P-loop is different. The new position creates a hydrophobic interaction with Arg748. (**b**) Comparison of the AMPPNP-binding pockets of the wild type (left) and the L858R mutant (right). The entrance to the ATP-binding site is more accessible, because of the conformational change of Phe723 in the L858R mutant, as compared with its position in the wild-type protein. (**c**) Detailed view of the reported structure of the inactive wild-type EGFR-TK complexed with Lapatinib (PDB code: 1xxk). Leu858 forms a hydrophobic core (yellow colored stick model) with residues contributed by the A-loop. The location of Gly719 is shown in a sphere representation.

sensitivities to gefitinib were significantly increased in all three EGFR mutants, as compared with the wild-type EGFR. The IC_{50} values, measured by quantifying the phosphorylation of the L858R and G719S mutants, were 2.6–3.2-fold less than that of the wild-type EGFR (Figure 6b), consistent with the previous report (Gilmer *et al*., 2008). Importantly, the IC_{50} of the F723A mutant was the lowest among the three EGFR mutants (~4.4-fold less than that of the wild type), supporting our hypothesis that the wider active site entrance contributes to the gefitinib sensitivity.

Discussion

Although previous studies showed that the distinct EGFR drug sensitive mutations differ markedly in

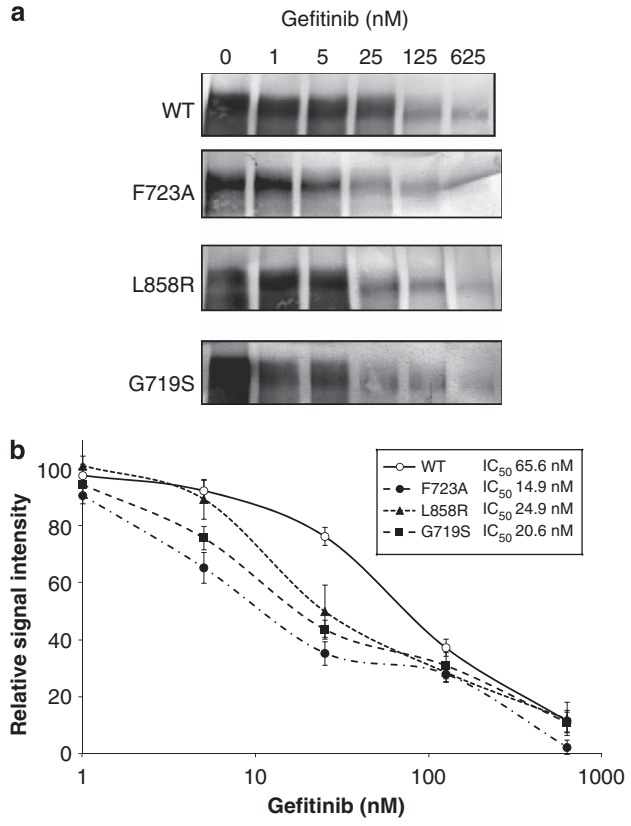

Figure 6 Inhibition of the wild-type and mutant EGFRs by increasing concentrations of gefitinib. (**a**) NIH3T3 cells retrovirally transferred with EGFRs were pre-treated with the indicated concentrations of gefitinib for 4 h, followed by stimulation with 10 ng/ml EGF for 10 min. Activation of EGFRs, as monitored by auto-phosphorylation (Tyr1173), is shown. Equal expression of EGFRs was confirmed by blotting with anti-EGFR antibodies (data not shown). (**b**) IC_{50}s were measured by quantifying the phosphorylation signals (*y* axis) in (**a**). The signal intensities of the phosphorylation without gefitinib treatment were set to 100.

Table 3 Enzyme kinetic parameters and inhibitor dissociation constants of the wild-type and mutant EGFR kinases

Kinase	$K_{m(ATP)}$ *(μM)*	k_{cat} *(s^{-1})*	k_{cat}/K_m *(μM/s)*	$K_{d(gefitinib)}$ *(nM)*
Wild type	21.0	0.185	0.00881	14.2
G719S	279.8	1.098	0.00392	31.9
G719S/T790M	45.9	0.409	0.00891	5.6

Abbreviation: EGFR, epidermal growth factor receptor.

qtheir inhibitor affinities and sensitivities, the structural reasons for these phenomena were elusive. In this study, we revealed the structural basis for the altered drug sensitivities caused by the distinct NSCLC-associated EGFR mutations, G719S, T790M and L858R.

The structure of the G719S single mutant was built without AMPPNP, due to ambiguous density in the binding site (Figure 3c). The weak electron density for AMPPNP in the G719S mutant structure is consistent with the kinetic analysis showing that the G719S single mutant displays 13.3-fold lower ATP-binding affinity as compared with the wild type (Table 3), as in the previous report (Yun *et al*., 2007). On the other hand, the electron density for AMPPNP in the G719S/T790M double mutant was well defined (Figure 3a). The conformation of the Met790 side chain in the G719S/T790M mutant is altered to optimize the AMPPNP binding, as compared with that of the Thr residue in the wild-type protein (Figures 4b and c), and is thus able to recover from the reduced ATP affinity produced by the G719S mutation (Table 3). Similarly, the introduction of a secondary T790M mutation in the L858R mutant, which normally displays reduced ATP-binding affinity, caused a significant increase in the affinity for ATP (Yun *et al*., 2008). Our G719S/T790M structure also showed that the T790M mutation strengthens the 'hydrophobic spine', thus confirming the mechanism of kinase activation predicted previously (Azam *et al*., 2008). Furthermore, the structure of the G719S/T790M mutant with gefitinib revealed that the G719S/T790M mutant can bind gefitinib in a similar manner to that previously observed for the wild type (Figure 4e). The results indicated that the resistance to gefitinib is not due to steric hindrance by the Met790 mutation. In fact, the Met790 residue shifts slightly in the gefitinib complex to adopt a position that optimizes gefitinib binding (Figure 4d), a modification also seen in the previously reported AEE788-bound T790M structure (Yun *et al*., 2008). Consistently, the G719S/T790M mutant binds gefitinib with increased affinity, as compared with the wild type and the G719S mutant (Table 3). Despite the increased gefitinib-binding affinity, the concurrent enhancement of ATP-binding affinity, caused by the T790M mutation in the G719S/T790M mutant, may render it resistant to gefitinib treatment. On the other hand, the T790M single mutation alone has a minimal effect on the affinity for ATP (Yun *et al*., 2008). Considering the results from our study (Table 3) and those reported previously (Yun *et al*., 2008), it is possible that the T790M mutation contributes to the tighter ATP binding more effectively in combination with other mutations, such as G719S and L858R, which confer decreased ATP-binding affinity.

We also identified the significant characteristics of the G719S and L858R mutant structures, which may explain the enhanced drug sensitivity of these mutants. The G719S mutant displays a slight upward shift in the P-loop (Figure 3c). We expect that this upward conformation of the P-loop would generate a binding site that not only displays greater accessibility to ATP-competitive inhibitors, but also releases ATP more easily. As TKIs, such as gefitinib, contain an aromatic substituent that binds deeply within the hydrophobic pocket at the back of the ATP-binding site (Stamos *et al*., 2002; Wood *et al*., 2004; Yun *et al*., 2007, 2008), we predict that the change in the binding site caused by the G719S mutation has less of an effect on the enzyme's binding affinity for TKIs, as compared with that for the smaller nucleotide ligands. In the L858R mutant, the A-loop is largely disordered and the Phe723 side chain adopts a novel conformation in which it rotates away from the binding pocket (Figure 5a). This movement

may explain the decreased ATP-binding affinity and increased gefitinib-binding affinity displayed by this drug-sensitive L858R mutant (Yun *et al*., 2007, 2008). We hypothesize that the wider active-site cleft of the L858R mutant may be responsible for its enhanced drug sensitivity. This hypothesis is supported by our *in vivo* analyses, which showed that the EGFR mutant, with the substitution of Ala for Phe at position 723, displays greatly enhanced sensitivity towards gefitinib (Figure 6b).

The structural variations adopted by the Met790 side chain in the G719S/T790M double mutant in complex with various ligands will provide important information for the development of more potent and selective drugs for use in resistant individuals.

Materials and methods

Protein expression and purification

The mutant bacmids of the EGFR kinase (residues 695–1022) were produced using a QuikChange site-directed mutagenesis kit (Stratagene, La Jolla, CA, USA). The baculoviruses for the His-tagged EGFR-TKs were created using the Bac-to-Bac Baculovirus Expression System (Invitrogen, Carlsbad, CA, USA), and were used to infect Sf9 cells. Cells were harvested 48 h after infection, and then disrupted by nitrogen cavitation. After centrifugation, the supernatant was loaded onto a Ni-NTA agarose column (QIAGEN, Valencia, CA, USA) and then the protein was eluted. The His-tag was cleaved by tobacco etch virus protease, and the protein was passed through the Ni-NTA agarose column again. The protein sample was further purified by Mono Q and Superdex 200 column chromatography (GE Healthcare, Buckinghamshire, UK) in a final buffer containing 20 mM Tris–HCl (pH 8.0), 150 mM NaCl, 2 mM DTT and 10% glycerol.

Enzyme kinetic assays and IC_{50} determinations

EGFR kinetic parameters were determined by using the ATP/NADH-coupled assay system, as described (Yun *et al*., 2007). The reaction mixture contained 4 mM $MnCl_2$, 1 mM phospho(enol)pyruvic acid trisodium salt hydrate), 1/50 of the final reaction mixture volume of the PK/LDH enzyme (pyruvate kinase/lactic dehydrogenase enzymes from rabbit muscle), 100 mg/ml poly-(Glu_4Tyr_1) peptide, 0.1 M 3-(*N*-morpholino)propanesulfonic acid (pH 7.5), 1 mM tris(2-carboxyethyl)phosphine, 0.2 mg/ml bovine serum albumin, 0.5 mM NADH, and 0.2–1 μM kinase. Various concentrations of ATP were added last, to start the reaction. Steady-state initial velocity data were drawn from the slopes of the A_{340} curves and fit to the Michaelis–Menten equation, to determine the V_m and K_m values.

Various amounts of gefitinib were added to the same kinase kinetic assays, except that the ATP concentration was fixed at 1 mM, to determine the range of gefitinib needed to encompass the IC_{50} values.

Binding constant assays

The equilibrium fluorescence quenching method was used to obtain the gefitinib binding constant, as described (Yun *et al*., 2007). The excitation and emission wavelengths were 283 nm and 340 nm, respectively. The gefitinib solution was titrated into the kinase solution in a buffer containing 20 mM Tris–HCl (pH 7.5), 250 mM NaCl, 0.5% glycerol and 1 mM tris(2-carboxyethyl)phosphine. The fluorescence data were fitted using the nonlinear curve-fitting program, KaleidaGraph (Synergy Software, Reading, PA, USA), and the dissociation constants (K_d) were determined as described (Yun *et al*., 2007).

Crystallization and data collection

For the crystallization of the wild-type and mutant EGFR-TKs complexed with AMPPNP, all proteins were mixed with 5 mM AMPPNP and 5 mM $MgCl_2$, and incubated at 4 °C for 6 h—overnight before crystallization. Diffraction quality crystals of the wild-type and G719S/T790M EGFR-TKs complexed with AMPPNP grew against a reservoir solution containing 0.2 M NaCl, 1 M sodium citrate and 0.1 M Tris–HCl buffer at pH 7.0, by the sitting drop vapor diffusion method. The crystals of the G719S mutant grew against a reservoir solution containing 1.1 M potassium sodium tartrate and 0.1 M MES buffer at pH 7.0, and the crystals of the L858R mutant grew against a reservoir solution containing 28% PEG300 and 0.1 M Tris–HCl buffer at pH 8.7, by the hanging drop vapor diffusion method.

The crystals of the G719S/T790M mutant complexed with gefitinib grew from the protein incubated with a final concentration of 0.5 mM gefitinib and 1% dimethyl sulfoxide overnight at 4 °C. This complex was incubated against a reservoir solution containing 1.1 M sodium citrate and 0.1 M MES buffer at pH 7.1, by the hanging drop vapor diffusion method.

The crystals of the apo G719S/T790M grew under microgravity by the counter-diffusion method (Garcia-Ruiz and Morena, 1994), using a JAXA Crystallization Box (JCB) at 20 °C. Capillaries were filled with protein solution and installed into a JCB syringe case filled with precipitant solution (1.7 M sodium citrate and 0.1 M MES buffer at pH 7.1). The Protein Crystallization Research Facility onboard 'Kibo' (Japanese experiment module) of the International Space Station was used for the space experiment.

All data were collected at 100 K, with reservoir solutions containing 16–30% glycerol as a cryoprotectant, as summarized in Tables 1 and 2. The diffraction data were processed with the XDS program (Kabsch, 1993) for the wild type, the MOSFLM program (Leslie, 1992) for the apo- and gefitinib-G719S/T790M, and the *HKL2000* program (Otwinowski and Minor, 1997) for the others.

Structure determination and refinement

All structures were solved by the molecular replacement method, using the programs MOLREP (Vagin and Teplyakov, 1997) and PHASER (Read, 2001), with the structure of the wild-type EGFR-TK (PDB code: 1M14, 2GS2 or 2GS6) as the search model. The model was corrected iteratively using the programs O (Jones *et al*., 1991) and Coot (Emsley and Cowtan, 2004), and the structure refinement was performed using the programs LAFIRE (Yao *et al*., 2006), REFMAC (Murshudov *et al*., 1997) and Crystallography & NMR System (Brunger *et al*., 1998). All refinement statistics are presented in Tables 1 and 2. The quality of the model was inspected by the program MolProbity (Davis *et al*., 2007). The graphic figures were created using the program PyMOL (DeLano, 2005). The superimposition was accomplished with the program lsqkab (Kabsch, 1976) in the CCP4 suite (Collaborative Computational Project, 1994).

Analysis of sensitivities of EGFR mutants to gefitinib

The full-length cDNAs encoding the wild-type and mutant EGFRs were cloned into the expression vector pMX-puro (Suzuki *et al*., 2002). Retroviral infection of NIH3T3 cells was performed as described (Suzuki *et al*., 2002). Infected cells were seeded in six-well plates at a concentration of 100 000 cells per

well. After an overnight incubation, the cells were pre-treated with 0–625 nM gefitinib for 4 h and then stimulated with 10 ng/ml EGF for 10 min. For the immunoblotting analysis, the proteins in the cell lysates were separated by 7.5% SDS–polyacrylamide gel electrophoresis and electrotransferred to polyvinylidene difluoride membranes (Immobilon, Millipore, Billerica, MA, USA). The membranes were incubated with anti-phospho EGFR (Tyr1173) rabbit polyclonal antibodies (Cell Signaling Technology, Beverly, MA, USA) and anti-EGFR rabbit polyclonal antibodies (Santa Cruz Biotechnology, Santa Cruz, CA, USA), followed by an anti-rabbit IgG $F(ab')_2$ conjugated with horseradish peroxidase. Specific bands were visualized with enhanced chemiluminescence (Renaissance, Perkin Elmer, Norwalk, CT, USA). Signals were quantified using Adobe Photoshop.

Conflict of interest

The authors declare no conflict of interest.

Acknowledgements

We thank C Takemoto, T Kaminishi, M Kawazoe, Y Fujii and S Kishishita for assisting with the data collection; Y Ishizuka-Katsura, R Akasaka, M Yamaguchi-Hirafuji, T Uchikubo-Kamo, A Urushibata and N Maoka for technical assistance; S Kusano for helpful assistance; and K Murayama for helpful advice. We also thank the beamline staffs of the X06SA (SLS), BL-5A (PF), BL41XU (SPring-8) and BL26B2 (SPring-8) beamlines. Portions of the data were collected at the Southeast Regional Collaborative Access Team (SER-CAT) 22-ID beamline at the Advanced Photon Source, Argonne National Laboratory. Supporting institutions may be found at http://www.ser.anl.gov/. Use of the Advanced Photon Source was supported by the US Department of Energy, Office of Science, Office of Basic Energy Sciences, under Contract No. W-31-109-Eng-38. This study was supported in part by the 'High-quality Protein Crystal Growth Experiment Project in JEM' promoted by the Japan Aerospace Exploration Agency. The Russian Spacecraft 'Progress' and 'Soyuz', provided by the Russian Federal Space Agency, were used for space transportation. A portion of the crystallization technology for the counter-diffusion method was developed by European Space Agency and University of Granada. This work was supported by the RIKEN Structural Genomics/Proteomics Initiative, the National Project on Protein Structural and Functional Analyses, the Targeted Proteins Research Program (TPRP), the Ministry of Education, Culture, Sports, Science and Technology of Japan, and by a Japanese Society for the Promotion of Science Fellowship (LJP).

References

Arteaga CL. (2002). Overview of epidermal growth factor receptor biology and its role as a therapeutic target in human neoplasia. *Semin Oncol* **29**: 3–9.

Azam M, Seeliger MA, Gray NS, Kuriyan J, Daley GQ. (2008). Activation of tyrosine kinases by mutation of the gatekeeper threonine. *Nat Struct Mol Biol* **15**: 1109–1118.

Brunger AT, Adams PD, Clore GM, DeLano WL, Gros P, Grosse-Kunstleve RW *et al*. (1998). Crystallography & NMR system: a new software suite for macromolecular structure determination. *Acta Crystallogr D Biol Crystallogr* **54**: 905–921.

Carmi C, Cavazzoni A, Vezzosi S, Bordi F, Vacondio F, Silva C *et al*. (2010). Novel irreversible epidermal growth factor receptor inhibitors by chemical modulation of the cysteine-trap portion. *J Med Chem* **53**: 2038–2050.

Cha MY, Lee KO, Kim JW, Lee CG, Song JY, Kim YH *et al*. (2009). Discovery of a novel Her-1/Her-2 dual tyrosine kinase inhibitor for the treatment of Her-1 selective inhibitor-resistant non-small cell lung cancer. *J Med Chem* **52**: 6880–6888.

Cha MY, Lee KO, Kim M, Song JY, Lee KH, Park J *et al*. (2011). Antitumor activity of HM781-36B, a highly effective pan-HER inhibitor in erlotinib-resistant NSCLC and other EGFR-dependent cancer models. *Int J Cancer* e-pub ahead of print 5 July 2011; doi: 10.1002/ijc.26276.

Collaborative Computational Project No.4 (1994). The CCP4 suite: programs for protein crystallography. *Acta Crystallogr D Biol Crystallogr* **50**: 760–763.

Davis IW, Leaver-Fay A, Chen VB, Block JN, Kapral GJ, Wang X *et al*. (2007). MolProbity: all-atom contacts and structure validation for proteins and nucleic acids. *Nucleic Acids Res* **35**: W375–W383.

de La Motte Rouge T, Galluzzi L, Olaussen KA, Zermati Y, Tasdemir E, Robert T *et al*. (2007). A novel epidermal growth factor receptor inhibitor promotes apoptosis in non-small cell lung cancer cells resistant to erlotinib. *Cancer Res* **67**: 6253–6262.

DeLano WL. (2005). *PyMOL v.0.98.*. DeLano Scientific: South San Francisco, CA.

Dixit A, Yi L, Gowthaman R, Torkamani A, Schork NJ, Verkhivker GM. (2009). Sequence and structure signatures of cancer mutation hotspots in protein kinases. *PLoS One* **4**: e7485.

Emsley P, Cowtan K. (2004). Coot: model-building tools for molecular graphics. *Acta Crystallogr D Biol Crystallogr* **60**: 2126–2132.

Engelman JA, Zejnullahu K, Gale CM, Lifshits E, Gonzales AJ, Shimamura T *et al*. (2007). PF00299804, an irreversible pan-ERBB inhibitor, is effective in lung cancer models with EGFR and ERBB2 mutations that are resistant to gefitinib. *Cancer Res* **67**: 11924–11932.

Garcia-Ruiz JM, Morena A. (1994). Investigations on protein crystal growth by the gel acupuncture method. *Acta Crystallogr D Biol Crystallogr* **50**: 484–490.

Gilmer TM, Cable L, Alligood K, Rusnak D, Spehar G, Gallagher KT *et al*. (2008). Impact of common epidermal growth factor receptor and HER2 variants on receptor activity and inhibition by lapatinib. *Cancer Res* **68**: 571–579.

Greulich H, Chen TH, Feng W, Janne PA, Alvarez JV, Zappaterra M *et al*. (2005). Oncogenic transformation by inhibitor-sensitive and -resistant EGFR mutants. *PLoS Med* **2**: e313.

Jiang J, Greulich H, Janne PA, Sellers WR, Meyerson M, Griffin JD. (2005). Epidermal growth factor-independent transformation of Ba/F3 cells with cancer-derived epidermal growth factor receptor mutants induces gefitinib-sensitive cell cycle progression. *Cancer Res* **65**: 8968–8974.

Jones TA, Zou JY, Cowan SW, Kjeldgaard M. (1991). Improved methods for building protein models in electron density maps and the location of errors in these models. *Acta Crystallogr A* **47**(Part 2): 110–119.

Kabsch W. (1976). A solution for the best rotation to relate two sets of vectors. *Acta Crystallogr A* **32**: 922–923.

Kabsch W. (1993). Automatic processing of rotation diffraction data from crystals of initially unknown symmetry and cell constants. *J Appl Cryst* **26**: 795–800.

Kobayashi N, Toyooka S, Soh J, Yamamoto H, Dote H, Kawasaki K *et al*. (2012). The anti-proliferative effect of heat shock protein 90 inhibitor, 17-DMAG, on non-small-cell lung cancers being resistant to EGFR tyrosine kinase inhibitor. *Lung Cancer* **75**: 161–166.

Kobayashi S, Boggon TJ, Dayaram T, Janne PA, Kocher O, Meyerson M *et al*. (2005). EGFR mutation and resistance of non-small-cell lung cancer to gefitinib. *N Engl J Med* **352**: 786–792.

Kornev AP, Haste NM, Taylor SS, Eyck LF. (2006). Surface comparison of active and inactive protein kinases identifies a conserved activation mechanism. *Proc Natl Acad Sci USA* **103**: 17783–17788.

Leslie AGW. (1992). *Joint CCP4 + ESF-EAMCB Newsletter on Protein Crystallography* **26**: 22–23.

Li D, Ambrogio L, Shimamura T, Kubo S, Takahashi M, Chirieac LR *et al*. (2008). BIBW2992, an irreversible EGFR/HER2 inhibitor highly effective in preclinical lung cancer models. *Oncogene* **27**: 4702–4711.

Liu Y, Shah K, Yang F, Witucki L, Shokat KM. (1998). A molecular gate which controls unnatural ATP analogue recognition by the tyrosine kinase v-Src. *Bioorg Med Chem* **6**: 1219–1226.

Lynch TJ, Bell DW, Sordella R, Gurubhagavatula S, Okimoto RA, Brannigan BW *et al*. (2004). Activating mutations in the epidermal growth factor receptor underlying responsiveness of non-small-cell lung cancer to gefitinib. *N Engl J Med* **350**: 2129–2139.

Mukohara T, Engelman JA, Hanna NH, Yeap BY, Kobayashi S, Lindeman N *et al*. (2005). Differential effects of gefitinib and cetuximab on non-small-cell lung cancers bearing epidermal growth factor receptor mutations. *J Natl Cancer Inst* **97**: 1185–1194.

Murshudov GN, Vagin AA, Dodson EJ. (1997). Refinement of macromolecular structures by the maximum-likelihood method. *Acta Crystallogr D Biol Crystallogr* **53**: 240–255.

Otwinowski Z, Minor W. (1997). Processing of X-ray diffraction data collected in oscillation mode. *Methods in Enzymol* **276**: 307–326.

Paez JG, Janne PA, Lee JC, Tracy S, Greulich H, Gabriel S *et al*. (2004). EGFR mutations in lung cancer: correlation with clinical response to gefitinib therapy. *Science* **304**: 1497–1500.

Pao W, Miller V, Zakowski M, Doherty J, Politi K, Sarkaria I *et al*. (2004). EGF receptor gene mutations are common in lung cancers from ″never smokers″ and are associated with sensitivity of tumors to gefitinib and erlotinib. *Proc Natl Acad Sci USA* **101**: 13306–13311.

Pao W, Miller VA, Politi KA, Riely GJ, Somwar R, Zakowski MF *et al*. (2005). Acquired resistance of lung adenocarcinomas to gefitinib or erlotinib is associated with a second mutation in the EGFR kinase domain. *PLoS Med* **2**: e73.

Read RJ. (2001). Pushing the boundaries of molecular replacement with maximum likelihood. *Acta Crystallogr D Biol Crystallogr* **57**: 1373–1382.

Shigematsu H, Gazdar AF. (2006). Somatic mutations of epidermal growth factor receptor signaling pathway in lung cancers. *Int J Cancer* **118**: 257–262.

Stamos J, Sliwkowski MX, Eigenbrot C. (2002). Structure of the epidermal growth factor receptor kinase domain alone and in complex with a 4-anilinoquinazoline inhibitor. *J Biol Chem* **277**: 46265–46272.

Suzuki T, J KT, Ajima R, Nakamura T, Yoshida Y, Yamamoto T. (2002). Phosphorylation of three regulatory serines of Tob by Erk1 and Erk2 is required for Ras-mediated cell proliferation and transformation. *Genes Dev* **16**: 1356–1370.

Taube E, Jokinen E, Koivunen P, Koivunen JP. (2011). A novel treatment strategy for EGFR mutant NSCLC with T790M-mediated acquired resistance. *Int J Cancer* e-pub ahead of print 27 September 2011; doi: 10.1002/ijc.26461.

Vagin A, Teplyakov A. (1997). MOLREP: an automated program for molecular replacement. *J Appl Cryst* **30**: 1022–1025.

Wakeling AE, Guy SP, Woodburn JR, Ashton SE, Curry BJ, Barker AJ *et al*. (2002). ZD1839 (Iressa): an orally active inhibitor of epidermal growth factor signaling with potential for cancer therapy. *Cancer Res* **62**: 5749–5754.

Wood ER, Truesdale AT, McDonald OB, Yuan D, Hassell A, Dickerson SH *et al*. (2004). A unique structure for epidermal growth factor receptor bound to GW572016 (Lapatinib): relationships among protein conformation, inhibitor off-rate, and receptor activity in tumor cells. *Cancer Res* **64**: 6652–6659.

Wu CH, Coumar MS, Chu CY, Lin WH, Chen YR, Chen CT *et al*. (2010). Design and synthesis of tetrahydropyridothieno[2,3-d]pyrimidine scaffold based epidermal growth factor receptor (EGFR) kinase inhibitors: the role of side chain chirality and Michael acceptor group for maximal potency. *J Med Chem* **53**: 7316–7326.

Yao M, Zhou Y, Tanaka I. (2006). LAFIRE: software for automating the refinement process of protein-structure analysis. *Acta Crystallogr D Biol Crystallogr* **62**: 189–196.

Yun CH, Boggon TJ, Li Y, Woo MS, Greulich H, Meyerson M *et al*. (2007). Structures of lung cancer-derived EGFR mutants and inhibitor complexes: mechanism of activation and insights into differential inhibitor sensitivity. *Cancer Cell* **11**: 217–227.

Yun CH, Mengwasser KE, Toms AV, Woo MS, Greulich H, Wong KK *et al*. (2008). The T790M mutation in EGFR kinase causes drug resistance by increasing the affinity for ATP. *Proc Natl Acad Sci USA* **105**: 2070–2075.

Zhang X, Gureasko J, Shen K, Cole PA, Kuriyan J. (2006). An allosteric mechanism for activation of the kinase domain of epidermal growth factor receptor. *Cell* **125**: 1137–1149.

Zhou W, Ercan D, Chen L, Yun CH, Li D, Capelletti M *et al*. (2009). Novel mutant-selective EGFR kinase inhibitors against EGFR T790M. *Nature* **462**: 1070–1074.

Zhou W, Ercan D, Janne PA, Gray NS. (2011). Discovery of selective irreversible inhibitors for EGFR-T790M. *Bioorg Med Chem Lett* **21**: 638–643.